Advances in Applied Mathematics and Mechanics
Adv. Appl. Math. Mech., Vol. **9**, No. 1, pp. 23-42

DOI: 10.4208/aamm.2014.m71
February 2017

Application of Modified Couple Stress Theory and Homotopy Perturbation Method in Investigation of Electromechanical Behaviors of Carbon Nanotubes

Mir Masoud Seyyed Fakhrabadi*

School of Mechanical Engineering, College of Engineering, University of Tehran, Tehran, Iran

Received 30 December 2014; Accepted (in revised version) 10 November 2015

Abstract. The paper presents the size-dependant behaviors of the carbon nanotubes under electrostatic actuation using the modified couple stress theory and homotopy perturbation method. Due to the less accuracy of the classical elasticity theorems, the modified couple stress theory is applied in order to capture the size-dependant properties of the carbon nanotubes. Both of the static and dynamic behaviors under static DC and step DC voltages are discussed. The effects of various dimensions and boundary conditions on the deflection and pull-in voltages of the carbon nanotubes are to be investigated in detail via application of the homotopy perturbation method to solve the nonlinear governing equations semi-analytically.

AMS subject classifications: 35Q70

Key words: Carbon nanotubes, modified couple stress theory, homotopy perturbation method, electrostatic actuation.

1 Introduction

Carbon nanotubes (CNTs) have found extensive potential and actual applications in high-level technologies ranging from medicine to engineering, since its discovery by Iijima in 1991 [1–5]. Due to the wide applications can be supposed for the CNTs in various conditions, many scientists have studied their different mechanical behaviors such as buckling loads or vibration properties. For example, Koochi et al. presented a new approach to model the buckling and stable length of multi-walled CNT probes near graphite sheets [6]. They applied a hybrid nano-scale continuum model based on Lennard-Jones potential to simulate the intermolecular force-induced deflection of the

*Corresponding author.
Email: mfakhrabadi@ut.ac.ir, msfakhrabadi@gmail.com (M. M. S. Fakhrabadi)

multi-walled CNTs and determined their stable lengths as a function of geometrical and material characteristics, initial gap and number of graphene layers.

In another research, Fakhrabadi et al. studied the vibrational behaviors of the CNTs using molecular mechanics and artificial neural network [7]. They applied molecular mechanics-based finite element method in order to compute the natural frequencies of the CNTs with various lengths and diameters and used the artificial neural network to predict the frequencies of the unmodeled CNTs. There can be found many other papers relating to the nano mechanical behaviors of the CNTs showing their capabilities to be utilized in various utilizations [8–10].

One of the main applications of the CNTs is in nano electromechanical systems (NEMS). NEMS are the miniaturized forms of the micro electromechanical systems (MEMS) composing of nano structures such as nano beams, shells, plates, tubes or other similar structures sensed or actuated electrically. Electrothermal, piezoelectric and electrostatic are more common actuation mechanisms in MEMS and NEMS [11–13]. But, the electrostatic actuation technique is more applicable than the others specially for actuation of the CNTs. Electrothermal actuators can produce high output force by low voltages, but the temperature generated by thermal actuator would be extremely high which can reach more than 800°C. The advantages of this actuator are that it can be fabricated easily; it can generate large force and deflection by low voltage and needs smaller chip area. But, the disadvantage is that the generated temperature is so high that it requires passive or active cooling system to reduce the temperature for certain applications of high bandwidth. The requirement to the effective powerful cooling systems in this actuation mechanism limits its application drastically, especially for the NEMS. Thus, for the system considered in this paper, it cannot be applied. On the other hand, piezoelectric actuation technique produces large forces and high power density, but the displacements generated are so small. In addition, there are some limitations in the piezoelectric actuators such as creep and hysteresis reducing the accuracy and high-frequency response capability of the actuators. The mentioned drawbacks do not allow us to apply it for the current case. Finally, in electrostatic actuation, the motion of electrodes is due to electrostatic repulsion by image charges mirrored in the ground plane beneath the suspended structure. This kind of actuator has small actuation energy and high frequency response, but it also has drawbacks such as high driving voltage and low output force. The advantages of this actuation approach make it an appropriate technique for the system studied in this paper and its shortages does not limit it. Because, for the current case, the nano system does not require larger forces and the actuation voltage can be appropriately provided.

NEMS in general and CNT-based NEMS in particular can possess applications in electronic circuits as nano switches, nano capacitors, nano resonators, nano transistors and elements of random access memories. All of the mentioned applications for the NEMS require high-precision conditions. Some experiments revealed that the classical elasticity theories may not have enough accuracy in predicting the mechanical behaviors of the micro and nano structures [14, 15]. Since continuum-mechanics has been widely applied in studying the mechanical and electromechanical behaviors of the micro and nano struc-

tures, scientists have made attempts to modify the available theories or develop some novel theorems to compensate the shortages of the classical elasticity. One of the effective theorems developed for this purpose is the modified couple stress theory (MCST) presented by Yang et al. [16].The classical couple stress elasticity theory presented and developed by Koiter, Toupin, Mindlin and Tiersten is a higher order continuum theory including four material constants (two classical and two additional) for isotropic elastic materials [17–20]. However, in the MCST, unlike the classical couple stress theory, the couple stress tensor is considered symmetric and only one internal material length scale parameter is involved. This theory has been applied in different researches regarding micromechanics and nanomechanics until now and the related papers are continuously published. However, it has not been applied to study the electromechanical behaviors of the CNTs yet.

Dequesnes et al. were the first research team studied the static pull-in behaviors of the CNTs under electrostatic actuation and van der Waals (vdW) force [21]. They applied a one DOF model in their research which was a simplification and might have some deviations from the real systems. In another research, Ke et al. presented two papers regarding the CNT-based NEMS [22, 23]. The first paper focused on the quality of charge distribution and the second one was about the stretching effects on doubly clamped CNTs. In addition, Ouakad and Younis studied the nonlinear dynamic behaviors of the CNTs under electrostatic actuation and presented the frequency response of the systems vs. different applied voltages [24].

In this paper, we are going to study the deflection, vibration and pull-in instability of the CNTs with different geometries and boundary conditions under electrostatic actuation. Because the governing equations, as presented in the following section, are nonlinear and may not be solved analytically by the common techniques, the numerical or some special analytic methods should be applied to analyze the mentioned phenomena in the CNTs. Of course, some semi-analytical methods were applied in order to investigate the mechanical and electromechanical properties of the nanostructures. For example, Soroush et al. studied the effects of Casimir and vdW forces on the pull-in instability of the cantilever nano beams using Adomian decomposition method (ADM) [25]. They applied this technique to obtain an analytical solution based on the distributed parameter model. In addition, Koochi et al. applied ADM to scrutinize the influences of surface effects including residual surface stress and surface elasticity on the size-dependent instability of the nano beams in the presence of Casimir force [26].

On the other hand, Abadyan et al. applied homotopy perturbation method to investigate the effects of Casimir force on the pull-in instability of the cantilever nano beams [27]. They studied the static pull-in of the nano beams using this method and compared the results with those in the literature. Although, this approach was applied in other researches to study the behaviors of the nanostructures [28, 29], it has not been used to investigate the electromechanical characterization of the CNTs under electrostatic actuation. Thus, He's homotopy perturbation method is to be applied in this paper [30]. This technique has some advantages rather than other common methods such as fast and safe conver-

gence. Moreover, it doesn't need to discretize the space and time domains unlike many other numerical techniques. It has less computational cost and does not require solving nonlinear discrete systems of differential equations.

2 Problem definition

This section provides the definition of the system under consideration. As shown in Fig. 1, suppose that a CNT is suspended over some graphene sheets with an initial gap equaling G_0 (state 1 in the figure). The CNT as the positive electrode and graphene sheets as the negative electrode (ground plate) are applied an electrical potential difference (V). The charge distributions over the electrodes make an attractive force between positive and negative charges. This force cooperated with the interatomic force between the electrodes lead to deflect the CNT towards the ground plate (state 2 in Fig. 1). The deflection value ($w = w(x)$ in Fig. 1) corresponds to the applied voltage up to where that the elastic force of the CNT cannot tolerate the attractive force resulted from the applied voltage and interatomic forces. Hence, it drops suddenly on the ground plate. This phenomenon is called pull-in instability and the corresponding voltage is pull-in voltage.

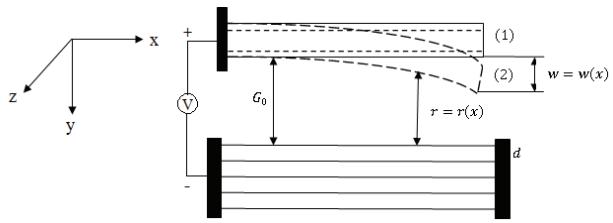

Figure 1: Schematic view of an electrostatically actuated carbon nanotube.

3 Mathematical formulation

Based on the MCST developed by Yang et al. the strain energy depends on the strain and curvature. The former corresponds to the classic stress and the latter relates to the couple stress. Hence, the strain energy U of an isotropic linear elastic material with volume Ω under an infinitesimal deformation can be formulated as Eq. (3.1)

$$U = \frac{1}{2}\iiint \Omega(\sigma : \varepsilon + m : \chi) dv, \tag{3.1}$$

where σ, ε, m and χ denote respectively the stress, strain, deviatoric part of couple stress and symmetric curvature tensors defined by Eqs. (3.2a)-(3.2d) [31]

$$\boldsymbol{\sigma} = \lambda tr(\boldsymbol{\varepsilon})\mathbf{I} + 2\mu\boldsymbol{\varepsilon}, \tag{3.2a}$$

$$\boldsymbol{\varepsilon} = \frac{1}{2}\left[(\nabla\mathbf{u}) + (\nabla\mathbf{u})^T\right], \tag{3.2b}$$

$$\mathbf{m} = 2l^2\mu\boldsymbol{\chi}, \tag{3.2c}$$

$$\boldsymbol{\chi} = \frac{1}{2}\left[(\nabla\boldsymbol{\theta}) + (\nabla\boldsymbol{\theta})^T\right], \tag{3.2d}$$

where λ and μ are Lame's constants and l, u and θ denote respectively the material length scale parameter, displacement vector and rotation vector. The latter is defined by Eq. (3.3)

$$\boldsymbol{\theta} = \frac{1}{2}curl(\mathbf{u}). \tag{3.3}$$

It is worth noting that both σ and m are symmetric, i.e., $\boldsymbol{\sigma} = \boldsymbol{\sigma}^T$ and $\mathbf{m} = \mathbf{m}^T$, due to the symmetry of $\boldsymbol{\varepsilon}$ and $\boldsymbol{\chi}$ in Eqs. (3.2b) and (3.2d). The material length scale parameter l is mathematically the square of the ratio of the modulus of curvature to the modulus of shear and is physically a property measuring the effect of couple stress [31].

Suppose that the x, y and z axes are as shown in Fig. 1. Then, the displacement field can be formulated as below:

$$u = u_0 - z\frac{\partial w(x)}{\partial x}, \quad v = 0, \quad w = w(x), \tag{3.4}$$

where u, v and w are respectively the displacements in x, y and z directions and u_0 is the midline stretching. By assuming small slopes in the EulerBernoulli beam as a model of the CNT after deformation but possible finite deflection w, the only non-zero component of the strain tensor considering the von-Karman nonlinearity for mid-plane stretching can be approximately expressed as:

$$\varepsilon_x = \frac{\partial u}{\partial x} + \frac{1}{2}\left(\frac{\partial w}{\partial x}\right)^2 = \frac{\partial u_0}{\partial x} - z\frac{\partial^2 w(x)}{\partial x^2} + \frac{1}{2}\left(\frac{\partial w}{\partial x}\right)^2. \tag{3.5}$$

For a slender beam with a large aspect ratio, the Poisson effect is secondary and can be disregarded to ease the formulation of the beam theory. Hence, the stress component in x direction is presented in Eq. (3.6) and the other components are considered zero

$$\sigma_x = E\varepsilon_x = E\left[\frac{\partial u_0}{\partial x} - z\frac{\partial^2 w(x)}{\partial x^2} + \frac{1}{2}\left(\frac{\partial w}{\partial x}\right)^2\right], \tag{3.6}$$

where E is the modulus of elasticity. Replacing Eq. (3.5) into Eqs. (3.2c)-(3.3) yield the non-zero components of $\boldsymbol{\theta}$, $\boldsymbol{\chi}$ and $\mathbf{m}$ as following:

$$\theta_y = -\frac{\partial w}{\partial x}, \quad \chi_{xy} = \chi_{yx} = -\frac{1}{2}\frac{\partial^2 w}{\partial x^2}, \quad m_{xy} = m_{yx} = -\mu l^2\frac{\partial^2 w}{\partial x^2}, \tag{3.7}$$

where μ is the shear modulus and the other components are zero. On the other hand, for the current case, the work done by the electrostatic force is expressed as:

$$W=\int_0^L q(x)w(x)dx, \tag{3.8}$$

where L is the length of the CNT. Substituting Eqs. (3.5)-(3.7) in Eq. (3.1) and applying the principle of minimum total potential energy, one can obtain the nonlinear partial differential equation governing the deflection of the doubly clamped CNTs as following:

$$(EI+\mu AI^2)\frac{\partial^4 w}{\partial x^4}-\Big(\frac{EA}{2L}\int_0^L\Big(\frac{\partial w}{\partial x}\Big)^2 dx\Big)\frac{\partial^2 w}{\partial x^2}=q(x), \tag{3.9}$$

where I is the moment of inertia, N is the external applied force and A is the cross-sectional area of the CNT. The paper presents the static and dynamic pull-in instabilities of the CNTs. The governing equations and solution methods of each item are presented respectively.

3.1 Static behavior

The deflection of the doubly clamped CNT applied an electrostatic voltage can be obtained from Eq. (3.9). The deflection can be obtained for the cantilevered CNTs using this equation with considering zero value for the second term. This can be attributed to this fact that mid-plane stretching does not appear in the linear behavior supposed for the CNTs with the cantilever boundary conditions. The maximum deflections of the cantilever and doubly clamped CNTs are respectively at the tip and longitudinal center.

The distributive force in the right hand of Eq. (3.9) composes of two parts: electrostatic actuation, q_{elec}, and vdW, q_{vdW}, interactions. The former is formulated in [21] as below

$$q_{elec}=\frac{\pi\varepsilon_0 V^2}{\sqrt{r(r+2R)}\ln^2\big[1+\frac{r}{R}+\sqrt{\frac{r(r+2R)}{R^2}}\big]}, \tag{3.10}$$

where ε_0, V, r and R, respectively denote electrical permittivity, voltage, gap and radius of the CNT. Using simplifications similar to those considered in [32], the above equation is written as following:

$$q_{elec}=\frac{\pi\varepsilon_0 V^2}{(r+R)\ln^2\big[\frac{2(r+R)}{R}\big]}. \tag{3.11}$$

According to Fig. 1, $r=G_0-w$, Hence, Eq. (3.11) can be rewritten as the following relation:

$$q_{elec}=\frac{\pi\varepsilon_0 V^2}{(G_0-w+R)\ln^2\big[\frac{2(G_0-w+R)}{R}\big]}. \tag{3.12}$$

On the other hand, vdW force of the system was presented in [21] and it can be formulated as below after the mentioned simplifications [6, 32]:

$$q_{vdw}=4\pi^2 c_6\sigma^2 d^2 N_w R\sum_{r=G_0}^{G_0+(N_G-1)d}\frac{1}{r^5}, \tag{3.13}$$

where c_6 and σ^2 are Lennard-Jones potential parameters describing vdW force and d, N_w and $\langle R\rangle$ represent distance between graphene sheets, number of graphene sheets and mean radius of the CNT.

By rewriting the above equation with respect to the deflection, we have

$$q_{vdw}=4\pi^2 c_6\sigma^2 d^2 N_w R\sum_{n=1}^{N_G}\frac{1}{\left(G_0+(n-1)d-w\right)^5}. \tag{3.14}$$

In order to solve the governing equations of the deflections of the CNTs under electrostatic actuation, it is better first to normalize the equations via considering the following nondimensional parameters:

$$\bar{w}=\frac{w}{G_0},\quad \bar{x}=\frac{x}{L},\quad \bar{R}=\frac{R}{G_0},\quad \bar{d}=\frac{d}{G_0}. \tag{3.15}$$

Replacing the above parameters in Eq. (3.9), we have

$$\begin{aligned}&\left(1+\frac{\alpha_0 l^2}{(d_o^2+d_i^2)}\right)\frac{d^4\bar{w}}{d\bar{x}^4}-\left(\alpha\int_0^1\left(\frac{d\bar{w}}{d\bar{x}}\right)^2 d\bar{x}\right)\frac{d^2\bar{w}}{d\bar{x}^2}\\ &=\frac{\beta V^2}{(1-\bar{w}+\bar{R})\ln^2\left[\frac{2(1-\bar{w}+\bar{R})}{\bar{R}}\right]}+\gamma\sum_{n=1}^{N_G}\frac{1}{\left(1+(n-1)\bar{d}-\bar{w}\right)^5},\end{aligned} \tag{3.16}$$

where d_i and d_0 are the inner and outer diameters of the CNT and,

$$\alpha_0=\frac{16\mu}{E}, \tag{3.17}$$

$\alpha=\frac{AG_0^2}{2I}$ for doubly clamped boundary conditions.

$\alpha=0$ for cantilever boundary conditions

$$\beta=\frac{\pi\varepsilon_0 L^4}{EIG_0^2},\quad \gamma=\frac{4\pi^2 c_6\sigma^2\bar{d}^2 N_w\bar{R}L^4}{EIG_0^3},$$

Eq. (3.17) is correct for the ignorable deflection of the graphene sheets in comparison to the deflection of the CNT. Thus, the graphene sheets are considered rigid bodies in

this study. Expansion theory is applied in this stage to solve the governing equations. Suppose that deflection can be formulated as below:

$$\bar{w}=\sum_{i=1}^{n}a_i\varphi_i(\bar{x}), \tag{3.18}$$

where a_i are the coefficients and $\varphi_i(x)$ are the shape modes. The shape modes corresponding to the cantilever and doubly clamped boundary conditions are presented in Eqs. (3.19a) and (3.19b), respectively,

$$\varphi(x)=\cosh\mu\bar{x}-\cos\mu\bar{x}-\frac{(\cosh\mu+\cos\mu)}{(\sinh\mu+\sin\mu)}(\sinh\mu\bar{x}-\sin\mu\bar{x}),\qquad \mu_{1st}=1.875, \tag{3.19a}$$

$$\varphi(x)=\cosh\lambda\bar{x}-\cos\lambda\bar{x}-\frac{(\cosh\lambda-\cos\lambda)}{(\sinh\lambda-\sin\lambda)}(\sinh\lambda\bar{x}-\sin\lambda\bar{x}),\qquad \lambda_{1st}=4.73. \tag{3.19b}$$

For static deflection of the CNT, the first mode is enough. By substituting the first term of Eq. (3.18) in Eq. (3.16), we have

$$\begin{aligned}&a\Big(1+\frac{\alpha_0 l^2}{(d_o^2+d_i^2)}\Big)\frac{d^4\varphi(\bar{x})}{d\bar{x}^4}-\alpha a^3\varphi''(\bar{x})\int_0^1\varphi'(\bar{x})^2d\bar{x}\\&=\frac{\beta V^2}{(1-a\varphi(\bar{x})+\bar{R})\ln^2\left[\frac{2(1-a\varphi(\bar{x})+\bar{R})}{\bar{R}}\right]}+\gamma\sum_{n=1}^{N_G}\frac{1}{(1+(n-1)\bar{d}-a\varphi(\bar{x}))^5}.\end{aligned} \tag{3.20}$$

Galerkin method is applied to Eq. (3.20) to solve it. By multiplying all of the terms with $\varphi(\tilde{x})$ and integrating over the domain, we can write

$$\begin{aligned}k_{1s}a+k_{2s}a^3-\int_0^1\frac{\beta V^2\varphi(\bar{x})}{(1-a\varphi(\bar{x})+\bar{R})\ln^2\left[\frac{2(1-a\varphi(\bar{x})+\bar{R})}{\bar{R}}\right]}d\bar{x}\\-\int_0^1\gamma\sum_{n=1}^{N_G}\frac{\varphi(\bar{x})}{(1+(n-1)\bar{d}-a\varphi(\bar{x}))^5}d\bar{x}=0,\end{aligned} \tag{3.21}$$

where

$$k_{1s}=\Big(1+\frac{\alpha_0 l^2}{(d_o^2+d_i^2)}\Big)\int_0^1\Big(\frac{d^2\varphi(\bar{x})}{d\bar{x}^2}\Big)^2d\bar{x},\quad k_{2s}=\alpha\Big(\int_0^1\varphi'(\bar{x})^2d\bar{x}\Big)^2. \tag{3.22}$$

Eq. (3.21) is the final governing formulae to analyze the static deflection of the CNT under electrostatic actuation using the MCST. It should be solved to obtain the deflection of the various CNTs vs. different applied voltages as well as the pull-in voltage corresponding to each case.

3.1.1 Homotopy perturbation method to solve static deflection

The homotopy perturbation method was applied before to analyze the electromechanical behavior of the CNTs based on classical elasticity theory [33]. In this paper, this technique is utilized in order to address and scrutinize the mentioned behaviors using a non-classical classical elasticity theory. Suppose that a nonlinear differential equation with given boundary conditions as Eq. (3.17) is to be solved [33, 34]

$$A(u)-f(r)=0, \qquad r\in\Omega, \tag{3.23a}$$

$$B\left(u,\frac{\partial u}{\partial n}\right)=0, \qquad r\in\Gamma, \tag{3.23b}$$

where A, u, $f(r)$, Ω, B, n, Γ denote respectively a general nonlinear operator, an unknown function, a given function of the variable r, problem domain, a given function for the boundaries, a given direction and domain boundaries. The general nonlinear operator may be divided into two linear, $L(u)$, and nonlinear, $N(u)$, parts. The main relation of the homotopy perturbation technique is presented below:

$$H(a,p)=L(a)-L(\bar{a})+p(N(a)+L(\bar{a}))=0, \tag{3.24}$$

where $\bar{a}$ is the initial guess satisfying the boundary conditions and a denotes the solution of the problem considered as below:

$$a=a_0+pa_1+p^2a_2+p^3a_3+p^4a_4+p^5a_5+\cdots. \tag{3.25}$$

Also, $p\in[0,1]$ is an embedding parameter. Its value equaling zero corresponds to the initial guess and equaling one corresponds to the solution of the problem. $N(a)$ can be expanded in Taylor series as presented below [33, 34]

$$\begin{aligned} N(a)=N(a_0)&+N'(a_0)(pa_1+p^2a_2+p^3a_3+p^4a_4+p^5a_5)\\ &+\frac{N''(a_0)}{2!}(pa_1+p^2a_2+p^3a_3+p^4a_4+p^5a_5)^2\\ &+\frac{N'''(a_0)}{3!}(pa_1+p^2a_2+p^3a_3+p^4a_4+p^5a_5)^3\\ &+\frac{N^{(4)}(a_0)}{4!}(pa_1+p^2a_2+p^3a_3+p^4a_4+p^5a_5)^4. \end{aligned} \tag{3.26}$$

Replacing Eq. (3.26) in Eq. (3.24), the coefficients of p^i, $i=1-5$ are obtained as presented below [33]

$$p^0: L(a_0)-L(\bar{a})=0, \tag{3.27a}$$

$$p^1: L(a_1)+N(a_0)+L(\bar{a})=0, \tag{3.27b}$$

$$p^2: L(a_2)+a_1N'(a_0)=0, \tag{3.27c}$$

$$p^3: L(a_3)+a_2N'(a_0)+a_1(N''(a_0))/2!=0, \tag{3.27d}$$

$$p^4: L(a_4)+a_3N'(a_0)+\frac{2a_1a_2}{2!}N''(a_0)+\frac{a_1^3}{3!}N'''(a_0)=0, \tag{3.27e}$$

$$p^5: L(a_5)+a_4N'(a_0)+\frac{2a_1a_3+a_2^2}{2!}N''(a_0)+\frac{3a_1^2a_2}{3!}N'''(a_0)+\frac{a_1^4}{4!}N^{(4)}(a_0)=0. \tag{3.27f}$$

For the current problem, according to Eq. (3.24), the linear and nonlinear parts are selected as below:

$$L(a)=k_{1s}a, \tag{3.28a}$$

$$N(a)=k_{2s}a^3-\int_0^1\frac{\beta V^2\varphi(\bar{x})}{(1-a\varphi(\bar{x})+\bar{R})\ln^2\left[\frac{2(1-a\varphi(\bar{x})+\bar{R})}{\bar{R}}\right]}d\bar{x}$$
$$-\int_0^1\gamma\sum_{n=1}^{N_G}\frac{\varphi(\bar{x})}{\left(1+(n-1)\bar{d}-a\varphi(\bar{x})\right)^5}d\bar{x}. \tag{3.28b}$$

3.1.2 Dynamic behavior

The size-dependent vibrational characteristics of the doubly clamped CNT applied a DC electrostatic voltage can be modeled using Eq. (3.9), if the inertia term is added,

$$(EI+\mu Al^2)\frac{\partial^4w}{\partial x^4}-\left(\frac{EA}{2L}\int_0^L\left(\frac{\partial w}{\partial x}\right)^2dx\right)\frac{\partial^2w}{\partial x^2}+m\frac{\partial^2w}{\partial t^2}=q_{elec}+q_{vdW}, \tag{3.29}$$

where m and t, are mass of the CNT per length and time, respectively. As mentioned before, the second term is considered zero for the cantilevered CNTs. The nondimensional parameters introduced in Eq. (3.15) as well as $\bar{t}=t/\sqrt{mL^4/EI}$ are applied to nondimensionalize Eq. (3.29). The final relation is presented in Eq. (3.30)

$$\left(1+\frac{\alpha_0l^2}{(d_o^2+d_i^2)}\right)\frac{\partial^4\bar{w}}{\partial\bar{x}^4}-\left(\alpha\int_0^1\left(\frac{\partial\bar{w}}{\partial\bar{x}}\right)^2d\bar{x}\right)\frac{\partial^2\bar{w}}{\partial\bar{x}^2}+\frac{\partial^2\bar{w}}{\partial\bar{t}^2}$$
$$=\frac{\beta V^2}{(1-\bar{w}+\bar{R})\ln^2\left[\frac{2(1-\bar{w}+\bar{R})}{\bar{R}}\right]}+\gamma\sum_{n=1}^{N_G}\frac{1}{\left(1+(n-1)\bar{d}-\bar{w}\right)^5}. \tag{3.30}$$

The Taylor expansion of the right hand terms of Eq. (3.30) are as following:

$$\frac{\beta V^2}{(1-\bar{w}+\bar{R})\ln^2\left[\frac{2(1-\bar{w}+\bar{R})}{\bar{R}}\right]}=A_1+A_2\bar{w}+A_3\bar{w}^2+\cdots, \tag{3.31a}$$

$$\gamma\sum_{n=1}^{N_G}\frac{1}{\left(1+(n-1)\bar{d}-\bar{w}\right)^5}=B_1+B_2\bar{w}+B_3\bar{w}^2+\cdots. \tag{3.31b}$$

The coefficients A_i and B_i are presented in Eqs. (3.32) and (3.33)

$$A_1=\frac{\beta V^2}{R^*\ln^2(a^*R^*)}, \tag{3.32a}$$

$$A_2=\frac{1}{\ln^2(a^*R^*)}\Big\{\frac{\beta V^2}{R^{*2}}+\frac{2\beta V^2}{R^{*2}\ln(a^*R^*)}\Big\}, \tag{3.32b}$$

$$A_3=\frac{1}{\ln^2(a^*R^*)}\Big\{\frac{\beta V^2}{R^{*3}}+\frac{2\beta V^2}{R^{*3}\ln(a^*R^*)}+\frac{\beta V^2(\ln(a^*R^*)+3)}{R^{*3}\ln(a^*R^*)^2}\Big\}, \tag{3.32c}$$

where $R^*=1+\bar{R}$ and $a^*=2/\bar{R}$. And

$$B_1=\sum_{n=1}^{N_G}\frac{\gamma}{d^{*5}},\quad B_2=\sum_{n=1}^{N_G}\frac{5\gamma}{d^{*6}},\quad B_3=\sum_{n=1}^{N_G}\frac{15\gamma}{d^{*7}}, \tag{3.33}$$

where $d^*=1+(n-1)\bar{d}$. Other A_i and B_i values are not presented here for brevity but can be easily obtained from successive differentiation. In addition, suppose that $C_i=A_i+B_i$. Substituting Eqs. (3.32), (3.33) and (3.34a) in Eq. (3.30) and using Galerkin method, we have the final governing equation in Eq. (3.34b)

$$\bar{w}=\sum_{i=1}^{n}u_i(t)\varphi_i(x), \tag{3.34a}$$

$$k_{1d}\frac{d^2u(t)}{dt^2}+k_{2d}u(t)+k_{3d}u^3(t)=k_{4d}+k_5du(t)+k_{6d}u^2(t)+\cdots, \tag{3.34b}$$

where

$$k_{1d}=\int_0^1\eta\varphi^2(x)dx, \tag{3.35a}$$

$$k_{2d}=\Big(1+\frac{\alpha_0 l^2}{(d_o^2+d_i^2)}\Big)\int_0^1\Big(\frac{d^2\varphi(x)}{dx^2}\Big)^2dx, \tag{3.35b}$$

$$k_{3d}=\Big[\int_0^1\alpha\Big(\frac{d\varphi(x)}{dx}\Big)^2dx\Big]^2, \tag{3.35c}$$

$$k_{4d}=C_1\int_0^1\varphi(x)dx, \tag{3.35d}$$

$$k_{5d}=C_2\int_0^1\varphi^2(x)dx, \tag{3.35e}$$

$$k_{6d}=C_3\int_0^1\varphi^3(x)dx. \tag{3.35f}$$

3.1.3 Homotopy perturbation method to solve dynamic deflection

To solve the governing equations of the size-dependent dynamic responses of the CNTs under applied step DC voltage, the homotopy perturbation technique is used. The nonlinear differential equation to be solved is presented in Eq. (3.36)

$$R(u(t))=0, \tag{3.36}$$

where R is the nonlinear operator and $u(t)$ is an unknown function [33,35]. Using $q\in[0,1]$ as an embedding parameter, the homotopy function can be written as Eq. (3.37):

$$H(\Phi,q)=(1-q)L[\Phi(t,q)-u_0(t)]-qR[\Phi(t,q),\Omega(q)]=0, \tag{3.37}$$

where $u_0(t)$ and L are respectively the initial guess satisfying the boundary conditions and non-zero auxiliary operator. As q increases from zero to one, $\Phi(t,q)$ changes from the initial guess $\Phi(t,0)=u_0(t)$ to the exact solution $\Phi(t,1)=u(t)$. Using Taylor expansion, $\Phi(t,q)$ can be expanded with respect to q as following [33,35]:

$$\Phi(t,q)=\Phi(t,0)+\lim_{n\to\infty}\sum_{j=1}^{n}\frac{1}{j!}\frac{\partial^j\Phi(t,q)}{\partial q^j}\Big|_{q=0}q^j=u_0(t)+\lim_{n\to\infty}\sum_{j=1}^{n}u_j(t)q^j, \tag{3.38}$$

where $u_j(t)$ is called jth-order deformation derivative. Solving Eq. (3.37), we can write:

$$(1-q)L[\Phi(t,q)-u_0(t)]=qR[\Phi(t,q),\Omega(q)], \tag{3.39a}$$

$$\Phi(0,q)=0,\quad \frac{d\Phi(0,q)}{dt}=0. \tag{3.39b}$$

If $q=0$, then Eq. (3.39a) turns to the following relation to obtain the zero-order deformation.

$$L[\Phi(t,0)-u_0(t)]=0. \tag{3.40}$$

Differentiating Eq. (3.39a) with respect to q and setting $q=0$, the first-order deformation relation with zero initial conditions can be obtained:

$$L[u_1(t)]=qR[\Phi(t,q),\Omega(q)]\Big|_{q=0}. \tag{3.41}$$

The jth order derivative of Eq. (3.39a) and setting $q=0$ results in the jth-order deformation equation [35]:

$$L[u_j(t)-\delta_j u_{j-1}(t)]=\frac{1}{(j-1)!}\frac{\partial^{j-1}R[\Phi(t,q),\Omega(q)]}{\partial q^{j-1}}\Big|_{q=0}, \tag{3.42}$$

where

$$\delta_j=\begin{cases}0, & \text{if } j\leq 1,\\ 1, & \text{otherwise.}\end{cases} \tag{3.43}$$

The higher-order approximations of the exact solution can be achieved via solving Eq. (3.42).

In this stage, the explained method is applied to solve the governing equations of the CNT vibration and dynamic pull-in under step DC voltage. Using a new time scale $\tau=\omega t$, Eq. (3.34b) can be rewritten as follows:

$$k_{1d}\omega^2\frac{d^2u(\tau)}{d\tau^2}+k_{2d}u(\tau)+k_{3d}u^3(\tau)-k_{4d}-k_{5d}u(\tau)-k_{6d}u^2(\tau)-\cdots=0. \tag{3.44}$$

The nonlinear and linear operators of Eq. (3.37) are defined as below [33]:

$$R[\Phi(\tau,q),\Omega(q)] = k_{1d}\omega(q)^2\frac{\partial^2\Phi(\tau,q)}{\partial\tau^2} + k_{2d}\Phi(\tau,q) + k_{3d}\Phi(\tau,q)^3 - k_{4d} - k_{5d}\Phi(\tau,q) - k_{6d}\Phi(\tau,q)^2 - \cdots, \tag{3.45a}$$

$$L[\Phi(t,q)] = \omega_0^2\Big(\frac{\partial^2\Phi(t,q)}{\partial\tau^2} + \Phi(t,q)\Big). \tag{3.45b}$$

The initial guess to the system deflection is considered $u_0(\tau) = 0$. Thus, the first order-approximation is obtained via solving Eq. (3.41):

$$u_1(t) = \frac{k_{4d}}{\omega_0^2}(1-\cos(\tau)). \tag{3.46}$$

The governing equation to the undamped vibration of the CNT should be expressed based on the following base functions:

$$\cos(m\tau) = 0, \quad m = 1,2,3,\cdots. \tag{3.47}$$

Hence, in order to eliminate the secular terms in the jth order approximation, the coefficients of $\cos(\tau)$ in the $(j-1)$th order deformation equation should be set zero. This fact results in an algebraic equation and its solution leads to $\omega_{(j-2)}$. The second order-approximation is obtained from solving Eq. (3.42).

$$u_2(\tau) = \frac{k_{1d}k_{4d}(1+k_1d)(1-\cos(\tau))}{k_{2d}+k_{5d}}, \qquad \omega_0 = \frac{\sqrt{k_{1d}(k_{2d}+k_{5d})}}{k_{1d}}. \tag{3.48}$$

Successive solution of Eq. (3.42) for higher-order approximations and setting $q=1$ results in more exact results according to Eq. (3.49)

$$u(\tau) = \sum_{j=0}^{n+2} u_j(t), \qquad \omega = \sum_{j=0}^{n}\omega_j. \tag{3.49}$$

4 Results and discussion

In this section, the results obtained from the developed governing equations and the formulations of the homotopy perturbation method are presented. The results include the static and dynamic deflections of the electrostatically actuated CNTs with different dimensions and boundary conditions in the presence of vdW effects as well as their pull-in voltages (both static and dynamic). They are computed using the MCST and are to be compared with the values estimated using the classical elasticity theories. The elastic modulus of the CNT is considered 1TPa. The constants of Lennard-Jones potential are assumed $c_6 = 2.43\times10^{-78}\text{Nm}^7$ and $\sigma = 1.14\times10^{29}\text{m}^{-3}$ [21] and the number of graphene sheets is $N_G = 30$. Other assumptions are presented in detail in the relative sub-sections. The dimensions relating to the studied CNTs are: length (L) equals 50nm, radius (R) is 6.785 and initial gap (G) equals 4nm.

4.1 Deflection of CNT under static voltage

Fig. 2(a) illustrates the tip deflection of the cantilevered CNT under different applied voltages. The results are presented for three length scale parameters. As shown in this figure, the tip deflection of the CNT increases with the increment in the voltage up to maximum value and then it suddenly drops down on the ground plate. This phenomenon is called static pull-in and the corresponding voltage, as described before, is the static pull-in voltage.

The figure shows that there is an initial deflection in the absence of the electrostatic actuation. This means that the cantilevered CNT shows initial deformation under vdW force. In addition, the figure reveals that application of the MCST results in higher pull-in voltages. This can be attributed to the fact that the MCST increases the stiffness of the CNT. Thus, the stiffer CNTs demand higher voltages to pull-in.

Fig. 2(b) depicts the center-pint deflection and static pull-in instability of the doubly clamped CNT vs. applied voltage. According to the figure, one may conclude that the doubly clamped CNT represents similar behavior to the cantilevered CNT with some special differences. The first difference relates to the initial deflection under only vdW interactions. As shown in the figure, initial deflection of the doubly clamped CNT is ignorable. This can be attributed to the stiffer structures of the doubly clamped CNTs in comparison to the cantilevered ones. In addition, the doubly clamped CNTs tolerate larger deformation than the cantilevered CNTs before pull-in. This fact has the reason similar to the previous case. Application of the MCST for the doubly clamped CNT, similar to the cantilevered CNT, results in larger pull-in voltages. The comparison between the pull-in voltages presented in Figs. 2(a) and (b) reveals that the doubly clamped CNTs have remarkably higher pull-in voltages than the cantilevered CNTs.

The effects of increasing length scale parameter on the static pull-in voltages of the cantilever and doubly clamped CNTs are respectively shown in Figs. 3(a) and (b). The figures prove that increasing length scale parameter increases the static pull-in voltages

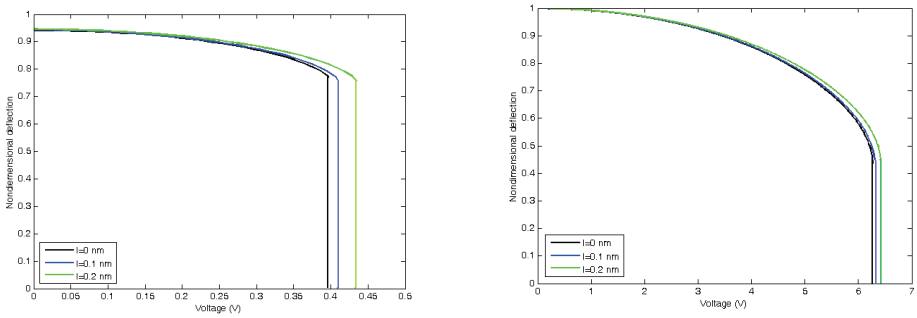

(a) (b)

Figure 2: (a) Tip deflection of the cantilevered CNT, (b) Center-point deflection of the doubly clamped CNT.

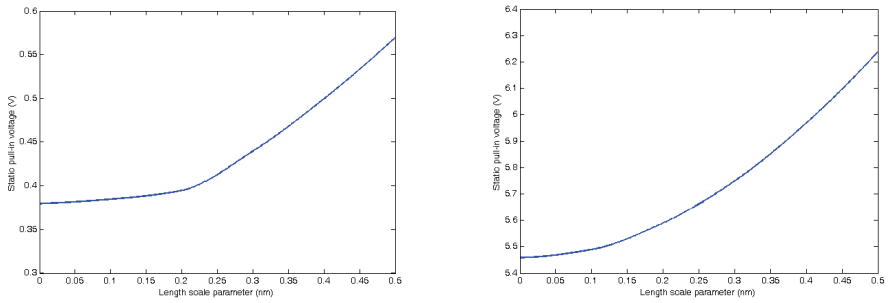

(a) (b)

Figure 3: Effects of increasing length scale parameter on static pull-in voltages of (a) cantilevered, (b) doubly clamped CNT.

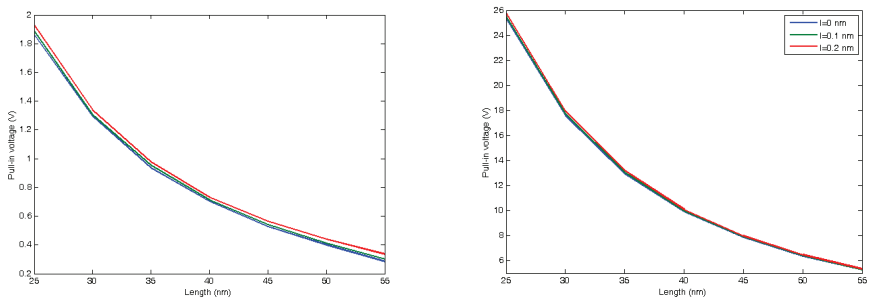

(a) (b)

Figure 4: Static pull-in voltages of the CNTs with (a) cantilever, (b) doubly clamped boundary conditions vs. length.

of the CNTs with both boundary conditions. It seems that the gradient of variations increases with increasing this parameter. This can be attributed to increasing the stiffness of the CNT with increasing the length scale parameter.

The effects of increasing length on the static pull-in voltages of the cantilever and doubly clamped CNTs are illustrated in Figs. 4(a) and (b). According to the figures, increasing length decreases the pull-in voltages of the CNTs with both boundary conditions. The reason is that increasing length weakens the nano structure and reduces its stiffness. Thus, longer CNTs have smaller pull-in voltages.

Figs. 5(a) and (b) respectively show the effects of radius variation on the static pull-in voltages of the cantilever and doubly clamped CNTs. The figures reveal that increasing radius increases the pull-in voltages of the CNT with both boundary conditions. This can be attributed to the fact that increasing radius strengthens the CNT and increases its stiffness. Thus, the CNTs with larger diameters have higher pull-in voltages. Moreover, the figures show that application of the MCST increases the pull-in voltages.

The effects of changes of gap distance between the electrodes on the static pull-in

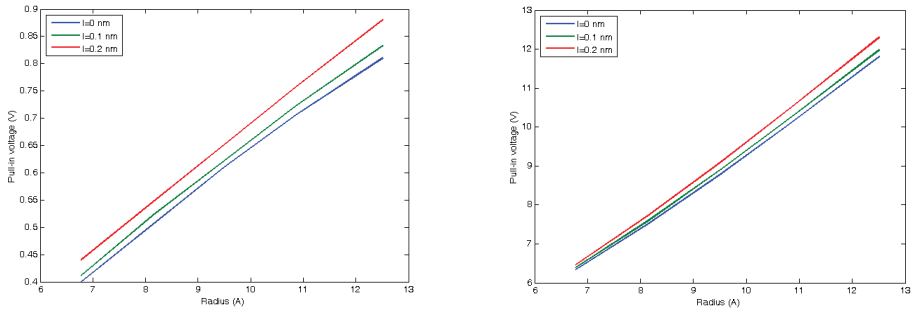

(a) (b)

Figure 5: Static pull-in voltages of the CNTs with (a) cantilever, (b) doubly clamped boundary conditions vs. radius.

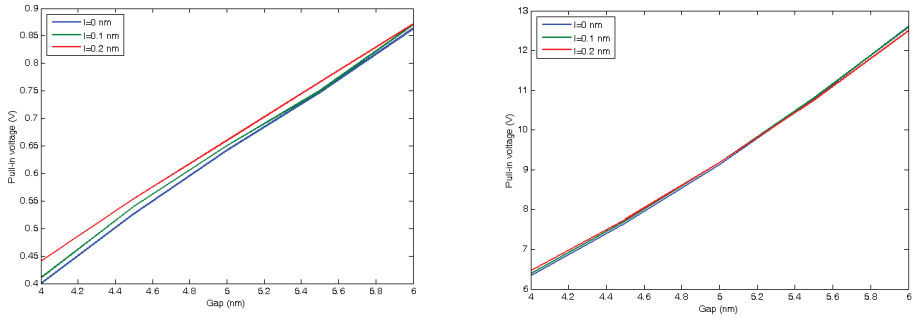

(a) (b)

Figure 6: Static pull-in voltages of the CNTs with (a) cantilever, (b) doubly clamped boundary conditions vs. gap.

voltages of the cantilever and doubly clamped CNTs are depicted in Figs. 6(a) and (b). According to the figures, increasing gap increases the pull-in voltages of the CNTs with the considered boundary conditions. The reason is that both of the vdW and electrostatic forces are gap-dependant loads. Thus, increasing gap weakens both of them. Hence, in order to reach the pull-in, higher voltages should be applied. Similar to the previous cases, Figs. 6(a) and (b) confirm that application of the MCST increases the pull-in voltages.

4.2 Analysis of CNTs under step DC actuation

The physical and geometrical conditions of the CNTs studied in this subsection are same as those in 2-1. The vibration of the CNTs with the cantilever and doubly clamped boundary conditions are illustrated in Figs. 7(a) and (b). According to the figure, the increment in the applied voltage results in the larger vibration amplitudes. This is correct for both

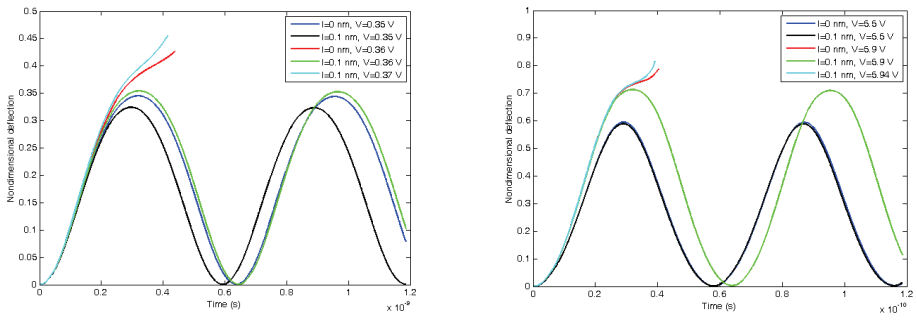

(a) (b)

Figure 7: Vibration of (a) cantilever, (b) doubly clamped CNTs under step DC voltages.

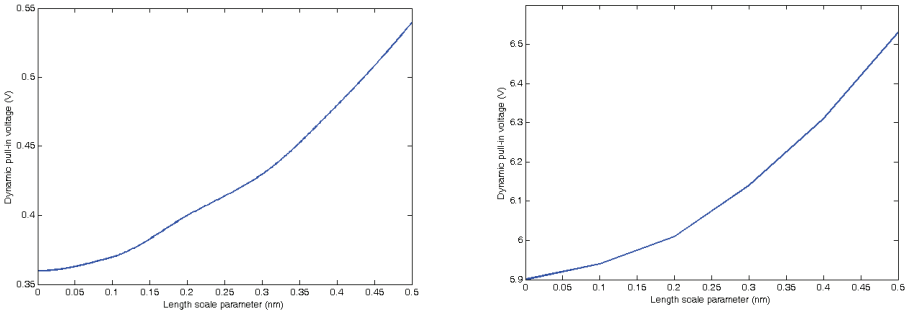

(a) (b)

Figure 8: Effects of various length scale parameters on dynamic pull-in voltages of the CNT with (a) cantilever, (b) doubly clamped boundary conditions.

boundary conditions. However, the increment of the vibration amplitude does not occur for any arbitrary DC voltage. When the voltage reaches to a threshold, the CNT does not follow the previous oscillatory motion and diverges from it. This is the dynamic pull-in and the corresponding voltage is the dynamic pull-in voltage. The figures reveal that application of the MCST increases the dynamic pull-in voltages, as well. Similar to the static pull-in voltages, the dynamic pull-in voltages of the doubly clamped CNTs are greatly larger than the dynamic pull-in voltages of the cantilevered CNTs with same dimensions.

Figs. 8(a) and (b) show the effects of changes in the length scale parameters on the dynamic pull-in voltages of the CNTs with the cantilever and doubly clamped boundary conditions. According to the figures, increasing length scale parameter increases the dynamic pull-in voltages of the CNTs with both boundary conditions, Similar to the static cases, this increment can be attributed to the stiffer nano structures obtained from application of the MCST.

5 Conclusions

The paper presented the static deflection and vibration of the CNTs under electrostatic actuation in the presence of vdW interactions using the MCST. The homotopy perturbation method was applied to investigate the effects of diameter, length and gap distance variations on the pull-in voltages of the CNTs with two cantilever and doubly clamped boundary conditions. The results proposed that the CNTs with longer lengths and smaller diameters failed to pull-in easier. On the other hand, pull-in phenomenon remarkably depended on the gap distance between the CNTs and substrate. Smaller gaps resulted in lower pull-in voltages. The results revealed that application of the MCST confined to stiffer CNTs with higher pull-in voltages. Increasing the length scale parameter increased both of the static and dynamic pull-in voltages.

References

[1] S. IIJIMA, *Helical microtubules of graphitic carbon,* Nature, 354(6348) (1991), pp. 56–58.
[2] M. SUNG, S.-U. PAEK, S.-H. AHN AND J. H. LEE, *A study of carbon-nanotube-based nanoelectromechanical resonators tuned by shear strain,* Comput. Mater. Sci., 51(1) (2012), pp. 360–364.
[3] O. LOH, X. WEI, J. SULLIVAN, L. E. OCOLA, R. DIVAN AND H. D. ESPINOSA, *Carbon-carbon contacts for robust nanoelectromechanical switches,* Adv. Mater., 24(18) (2012), pp. 2463–2468.
[4] C. L. CHENG AND G. J. ZHAO, *Steered molecular dynamics simulation study on dynamic self-assembly of single-stranded DNA with double-walled carbon nanotube and graphene,* Nanoscale, 4(7) (2012), pp. 2301–2305.
[5] S. ADHIKARI AND R. CHOWDHURY, *The calibration of carbon nanotube based bionanosensors,* J. Appl. Phys., 107(12) (2010), pp. 124322–124322.
[6] A. KOOCHI, A. S. KAZEMI, A. NOGHREHABADI, A. YEKRANGI AND M. ABADYAN, *New approach to model the buckling and stable length of multi walled carbon nanotube probes near graphite sheets,* Mater. Design, 32(5) (2011), pp. 2949–2955.
[7] M. M. S. FAKHRABADI, M. SAMADZADEH, A. RASTGOO, M. H. YAZDI AND M. M. MASHHADI, *Vibrational analysis of carbon nanotubes using molecular mechanics and artificial neural network,* Physica E: Low-Dimensional Systems and Nanostructures, 44(3) (2011), pp. 565–578.
[8] M. M. S. FAKHRABADI, A. AMINI, F. RESHADI, N. KHANI AND A. RASTGOO, *Investigation of buckling and vibration properties of hetero-junctioned and coiled carbon nanotubes,* Comput. Mater. Sci., 73 (2013), pp. 93–112.
[9] X. HUANG, H. YUAN, W. LIANG AND S. ZHANG, *Mechanical properties and deformation morphologies of covalently bridged multi-walled carbon nanotubes: multiscale modeling,* J. Mech. Phys. Solids, 58(11) (2010), pp. 1847–1862.
[10] S. C. PRADHAN AND T. MURMU, *Small-scale effect on vibration analysis of single-walled carbon nanotubes embedded in an elastic medium using nonlocal elasticity theory,* J. Appl. Phys., 105(12) (2009), pp. 124306–124306.
[11] R. ANSOLA, E. VEGUERÍA, J. CANALES AND C. ALONSO, *Evolutionary optimization of compliant mechanisms subjected to non-uniform thermal effects*, J. Finite. Elements. Anal. Design, 57 (2012), pp. 1–14.

[12] S. TAYYABA, N. AFZULPURKAR AND M. W. ASHRAF, *Simulation and design optimization of piezoelectricaly actuated valveless blood pump for hemofiltration system*, J. Sens. Transducers., 139 (2012), pp. 63–78.
[13] M. M. ZAND, *The dynamic pull-in instability and snap-through behavior of initially curved microbeams*, J. Mech. Adv. Mat. Struct., 19 (2012), pp. 485–491.
[14] J. S. STÖLKEN AND A. G. EVANS, *A microbend test method for measuring the plasticity length scale,* Acta Materialia, 46(14) (1998), pp. 5109–5115.
[15] R. MINDLIN AND H. TIERSTEN, *Effects of couple-stresses in linear elasticity,* Archive Rat. Mech. Anal., 11(1) (1962), pp. 415–448.
[16] F. YANG, A. C. M. CHONG, D. C. C. LAM AND P. TONG, *Couple stress based strain gradient theory for elasticity,* Int. J. Solids Structures, 39(10) (2002), pp. 2731–2743.
[17] W. T. KOITER, *Couple stresses in the theory of elasticity, I and II,* Nederl. Akad. Wetensch. Proc. Ser. B, 67 (1964), pp. 17–29.
[18] R. A. TOUPIN, *Elastic materials with couple-stresses,* Archive Rat. Mech. Anal., 11(1) (1962), pp. 385–414.
[19] R. D. MINDLIN, *Influence of couple-stresses on stress concentrations,* Exp. Mech., 3(1) (1963), pp. 1–7.
[20] R. D. MINDLIN AND H. F. TIERSTEN, *Effects of couple-stresses in linear elasticity,* Archive Rat. Mech. Anal., 11(1) (1962), pp. 415–448.
[21] M. DEQUESNES, S. V. ROTKIN AND N. R. ALURU, *Calculation of pull-in voltages for nanoelectromechanical switches,* J. Nanotech., 13 (2002), pp. 120–131.
[22] C. KE AND H. D. ESPINOSA, *Numerical analysis of nanotube based NEMS devices–part I: electrostatic charge distribution on multiwalled nanotubes*, J. Appl. Mech., 72 (2005), pp. 721–725.
[23] C. KE, H. D. ESPINOSA AND N. PUGNO, *Numerical analysis of nanotube based NEMS devices–part II: role of finite kinematics, stretching and charge concentration*, J. Appl. Mech., 72 (2005), pp. 726–731.
[24] H. M. OUAKAD AND M. I. YOUNIS, *Nonlinear dynamics of electrically actuated carbon nanotube resonators,* J. Comput. Nonlinear Dyn., 5 (2010), pp. 1–13.
[25] R. SOROUSH, A. KOOCHI, A. S. KAZEMI, A. NOGHREHABADI, H. HADDADPOUR AND M. ABADYAN, *Investigating the effect of Casimir and van der Waals attractions on the electrostatic pull-in instability of nano actuators*, J. Phys. Scr., 82 (2010), 045801.
[26] A. KOOCHI, A. KAZEMI, F. KHANDANI AND M. ABADYAN, *Influence of surface effects on size-dependent instability of nano-actuators in the presence of quantum vacuum fluctuations,* J. Phys. Scr., 85 (2012), 035804.
[27] M. ABADYAN, A. NOVINZADEH AND A. KAZEMI, *Approximating the effect of the Casimir force on the instability of electrostatic nano-cantilevers*, J. Phys. Scr., 81 (2010), 015801.
[28] A. KOOCHI, A. NOGHREHABADI, M. ABADYAN AND E. ROOHI, *Approximating the effect of van der Waals force on the instability of electrostatic nano-cantilevers*, Int. J. Modern Phys. B, 25(29) (2011), pp. 3965–3976.
[29] J. ABDI, A. KOOCHI, A. S. KAZEMI AND M. ABADYAN, *Modeling the effects of size dependence and dispersion forces on the pull-in instability of electrostatic cantilever NEMS using modified couple stress theory,* Smart Mater. Struct., 20 (2011), 055011.
[30] J. H. HE, *Homotopy perturbation technique,* Comput. Methods Appl. Mech. Eng., 178(3) (1999), pp. 257–262.
[31] F. YANG, A. C. M. CHONG, D. C. C. LAM AND P. TONG, *Couple stress based strain gradient theory for elasticity,* Int. J. Solids Struct., 39(10) (2002), pp. 2731–2743.
[32] C. H. KE, N. PUGNO, B. PENG AND H. D. ESPINOSA, *Experiments and modeling of carbon*

nanotube-based NEMS devices, J. Mech. Phys. Solids, 53(6) (2005), pp. 1314–1333.

[33] M. M. S. FAKHRABADI, A. RASTGOO AND M. T. AHMADIAN, *Analysis of pull-in instability of electrostatically actuated carbon nanotubes using the homotopy perturbation method,* J. Mech. Mater. Struct., 8(8) (2013), pp. 385–401.

[34] M. MOJAHEDI, M. M. ZAND AND M. T. AHMADIAN, J. Appl. Math. Model., 34 (2010), pp. 1032–1041.

[35] M. MOGHIMI ZAND AND M. T. AHMADIAN, *Application of homotopy analysis method in studying dynamic pull-in instability of microsystems,* Mech. Res. Commun., 36(7) (2009), pp. 851–858.